Reduced density-matrix functionals applied to the Hubbard dimer

Ebad Kamil,[1] Robert Schade,[2] Thomas Pruschke,[1] and Peter E. Blöchl[2,3]

[1]*Institute for Theoretical Physics, Georg-August-Universität Göttingen, Friedrich-Hund-Platz 1, 37077 Göttingen, Germany*
[2]*Institute for Theoretical Physics, Clausthal University of Technology, Leibnizstr. 10, 38678 Clausthal-Zellerfeld, Germany*
[3]*Institute for Materials Physics, Georg-August-Universität Göttingen, Friedrich-Hund-Platz 1, 37077 Göttingen, Germany*

(Received 7 September 2015; revised manuscript received 7 December 2015; published 29 February 2016)

Common density-matrix functionals, the Müller and the power functional, have been benchmarked for the half-filled Hubbard dimer, which allows us to model the bond dissociation problem and the transition from the weakly to the strongly correlated limit. Unbiased numerical calculations are combined with analytical results. Despite the well known successes of the Müller functional, the ground state is degenerate with a one-dimensional manifold of ferromagnetic solutions. The resulting infinite magnetic susceptibility indicates another qualitative flaw of the Müller functional. The derivative discontinuity with respect to particle number is not present indicating an incorrect metal-like behavior. The power functional actually favors the ferromagnetic state for weak interaction. Analogous to the Hartree-Fock approximation, the power functional undergoes a transition beyond a critical interaction strength, in this case, however, to a noncollinear antiferromagnetic state.

DOI: 10.1103/PhysRevB.93.085141

I. INTRODUCTION

Ab initio calculations are dominated by density functional theory (DFT) [1,2], which provides an efficient and accurate description of the electronic structure for most materials [3]. For materials with strong correlations, however, many of the available density functionals yield poor results [4,5]. Most well known is the case of transition metal oxides, for which most density functionals produce a qualitatively incorrect description [6]. However, elementary chemical processes such as bond dissociation are also described poorly by currently available density functionals [5].

There is a quest to improve the description by borrowing from methods specifically designed for strongly correlated materials. Among them are LDA+U [7], DFT-plus-dynamical mean-field theory [8–10], and DFT-plus-Gutzwiller approximation [11–13]. The guiding idea behind these approaches is to merge density functional theory with methods developed for the study of strong correlations for model Hamiltonians such as the Hubbard model [14–16].

We consider reduced density-matrix functional theory (rDMFT) [17,18] to be a useful framework for a rigorous formulation of such hybrid theories [19,20]. Reduced density-matrix functional theory can be viewed as a relative of DFT, which emphasizes orbital occupations rather than the density as basic variable. Such a description seems to be natural for correlated materials, because the latter are dominated by orbital physics.

The link from rDMFT to many-particle wave functions has been established by Levy's constrained-search algorithm [18] on the one hand. The link to many-body perturbation theory and Green's function, on the other hand, has been provided recently [20] via the Luttinger-Ward functional [21].

In order to avoid the full complexity of an explicit many-body description, most density-matrix functionals are not extracted from the exact expressions [18,20]. Rather, one proceeds analogously to the development of density functionals, namely by searching models [22–26] for the density-matrix functional that capture the most essential physical effects while having an algebraic dependence on the density matrix.

The development of such model density-matrix functionals relies on benchmark systems that allow one to evaluate their quality. Of particular interest are exactly solvable problems. Such studies have been performed for the Moshinsky atom [27], the homogeneous electron gas [28], and the Hubbard model [29,30]. Di Sabatino *et al.* [30] performed an in-depth analysis of the method proposed by Sharma *et al.* [31] to evaluate the spectral function of the Hubbard dimer from the Müller density-matrix functional [22].

As pointed out by Cohen, Sanchez, and Yang [5], many of the failures of current density functionals for correlated materials can be traced back to the derivative discontinuities present in a surprisingly simple system, namely the hydrogen or helium dimer in different charge states, i.e., H_2^+, H_2, He_2^+. Therefore, the two-site Hubbard model, the Hubbard dimer, can be considered as a model system for the correlation effects present in a chemical bond.

The most prominent failure of density functionals occurs during bond dissociation. If we denote the hopping parameter between the bonded atoms with t and the on-site interaction strength with U, bond dissociation is described by the limit $t \to 0$ at constant U. Thus, the system evolves from a weakly correlated state into the strongly correlated limit $U/t \to \infty$ as the bond is broken. The large-interaction limit $U \to \infty$ of the Hubbard model differs from the bond-dissociation limit only by the choice of the energy scale.

One of the major arguments in favor of density-matrix functionals is that one of the most simple functionals, the Müller functional [22], seems to provide a correct description of the bond-dissociation problem, for which common density functionals fail [32]. In this paper we study the performance of a class of commonly used model density-matrix functionals for the half-filled Hubbard dimer. We point out that, despite some successes, also these density-matrix functionals reproduce a number of features in a qualitatively incorrect manner. Thus, this work sets the stage for the development of an entirely new class of functionals [20].

In Sec. II, we define our notation and introduce the basic concepts of density-matrix functionals. In Sec. III, we present the analytically exact treatment of the Hubbard dimer and describe its relevant properties. In Sec. IV, we describe the numerical methodology of searching for the ground state for the model density-matrix functionals. In Sec. V, we describe the results obtained with the Hartree-Fock approximation and the commonly used Müller and power functionals. In Sec. VI we study the Hubbard dimer beyond half filling, and in Sec. VII we discuss briefly the transferability of our results to larger systems. Our results are summarized in Sec. VIII.

II. THEORETICAL FRAMEWORK

A. General many-particle problem

The many-particle Hamiltonian for interacting electrons can be expressed in terms of field operators $\hat{\psi}(\vec{x})$ and $\hat{\psi}^\dagger(\vec{x})$ in the form

$$\begin{aligned}\hat{H} = &\int d^4x\ \hat{\psi}^\dagger(\vec{x})\left(\frac{-\hbar^2}{2m_e}\vec{\nabla}^2 + v_{\text{ext}}(\vec{x})\right)\hat{\psi}(\vec{x}) \\ &+ \frac{1}{2}\int d^4x \int d^4x'\ \hat{\psi}^\dagger(\vec{x})\hat{\psi}^\dagger(\vec{x'}) \\ &\times \frac{e^2}{4\pi\epsilon_0|\vec{r}-\vec{r'}|}\hat{\psi}(\vec{x'})\hat{\psi}(\vec{x}),\end{aligned} \tag{1}$$

where $\vec{x} = (\vec{r},\sigma)$ is a combined position and spin variable. We use the shorthand $\int d^4x = \sum_\sigma \int d^3x$ for the integration over positions and the sum over spin indices. The field operators obey the usual anticommutator relations $[\hat{\psi}^\dagger(\vec{x}),\hat{\psi}(\vec{x'})]_+ = \delta(\vec{r}-\vec{r'})\delta_{\sigma,\sigma'}$.

A discrete, orthonormal one-particle basis set $\{\chi_\alpha(\vec{x})\}$ determines the creation and annihilation operators of electrons in the one-particle orbitals

$$\begin{aligned}\hat{c}^\dagger_\alpha &= \int d^4x\ \chi_\alpha(\vec{x})\hat{\psi}^\dagger(\vec{x}) \\ \hat{c}_\alpha &= \int d^4x\ \chi^*_\alpha(\vec{x})\hat{\psi}(\vec{x}).\end{aligned} \tag{2}$$

In this one-particle basis set we obtain the discrete Hamiltonian

$$\hat{H} = \sum_{\alpha\beta} h_{\alpha\beta}\hat{c}^\dagger_\alpha\hat{c}_\beta + \frac{1}{2}\sum_{\alpha\beta\gamma\delta} U_{\alpha\beta\gamma\delta}\,\hat{c}^\dagger_\alpha\hat{c}^\dagger_\beta\hat{c}_\delta\hat{c}_\gamma \tag{3}$$

with the one-particle Hamiltonian

$$h_{\alpha,\beta} = \int d^4x\ \chi^*_a(\vec{x})\left(\frac{-\hbar^2}{2m_e}\vec{\nabla}^2 + v_{\text{ext}}(\vec{x})\right)\chi_\beta(\vec{x}). \tag{4}$$

The off-diagonal elements of $\boldsymbol{h}$ are named hopping parameters, and the diagonal elements are named orbital energies.

The interaction matrix elements are

$$U_{\alpha\beta\gamma\delta} = \int d^4x \int d^4x'\ \frac{e^2\chi^*_\alpha(\vec{x})\chi^*_\beta(\vec{x'})\chi_\gamma(\vec{x})\chi_\delta(\vec{x'})}{4\pi\epsilon_0|\vec{r}-\vec{r'}|}. \tag{5}$$

B. One-particle reduced density matrix

The one-particle reduced density matrix of an ensemble of fermionic many-particle wave functions $|\Phi_j\rangle$ with probabilities P_j is defined as

$$\rho_{\alpha\beta} = \sum_j P_j\langle\Phi_j|\hat{c}^\dagger_\beta\hat{c}_\alpha|\Phi_j\rangle. \tag{6}$$

The density matrix is often represented by the eigenvalues and eigenstates of the corresponding one-particle operator

$$\hat{\rho} = \sum_{\alpha\beta}|\chi_\alpha\rangle\rho_{\alpha,\beta}\langle\chi_\beta|. \tag{7}$$

The eigenvalues of $\hat{\rho}$ are the occupations f_n and the eigenstates $|\phi_n\rangle$ are named natural orbitals [33]. Thus the density matrix can be expressed by its eigenvalues and eigenstates in the form

$$\rho_{\alpha,\beta} = \sum_n\langle\chi_\alpha|\phi_n\rangle f_n\langle\phi_n|\chi_\beta\rangle. \tag{8}$$

Not every hermitian matrix can also be represented as the one-particle reduced density matrix of an ensemble of many-particle wave functions according to Eq. (6). A matrix that can be represented by an ensemble of fermionic N-particle wave functions is called ensemble N representable. Coleman [34] has shown that eigenvalues of all ensemble N-representable one-particle reduced density matrices lie between zero and one and that all hermitian matrices with eigenvalues between zero and one are ensemble N representable.

C. Helmholtz potential and density-matrix functional

The Helmholtz potential $A_{\beta,\mu}[\hat{H}]$, the thermodynamic potential for finite temperature and fixed particle number, for a many-particle system can be expressed with the help of the density-matrix functional $F^{\hat{W}}_\beta[\boldsymbol{\rho}]$ as [18,20,35,36]

$$\begin{aligned}&A_{\beta,N}[\hat{h}+\hat{W}] \\ &= \min_{|\phi_n\rangle,\,f_n\in[0,1]}\ \text{stat}_{\Lambda,\mu}\left\{\sum_n f_n\langle\phi_n|\hat{h}|\phi_n\rangle + F^{\hat{W}}_\beta\left[\sum_n|\phi_n\rangle f_n\langle\phi_n|\right]\right. \\ &\left.-\mu\left(\sum_n f_n - N\right) - \sum_{m,n}\Lambda_{m,n}\left(\langle\phi_n|\phi_m\rangle - \delta_{m,n}\right)\right\}\end{aligned} \tag{9}$$

where $\hat{h} = \sum_{\alpha,\beta}|\chi_\alpha\rangle h_{\alpha,\beta}\langle\chi_\beta|$.

The reduced density-matrix functional $F^{\hat{W}}_\beta[\boldsymbol{\rho}]$ is universal in the sense that it depends only on the intrinsic properties of the electron gas, namely the interaction $\hat{W}$, while it is independent of the one-particle Hamiltonian $\hat{h}$. The chemical potential μ is a Lagrange multiplier that constrains the electron number to N. Λ_{mn} are the Lagrange multipliers which enforce that natural orbitals $|\phi_m\rangle$ remain orthonormal. The reduced density-matrix functional

$$F^{\hat{W}}_\beta[\boldsymbol{\rho}] = E_H[\boldsymbol{\rho}] + U_{xc,\beta}[\boldsymbol{\rho}] \tag{10}$$

is the sum of Hartree energy E_H and the exchange-correlation energy U_{xc}.

The Hartree energy $E_H[\boldsymbol{\rho}]$ is obtained from the electron density

$$n(\vec{r}) = \sum_\sigma\sum_{\alpha,\beta}\chi_\alpha(\vec{r},\sigma)\rho_{\alpha,\beta}\chi^*_\beta(\vec{r},\sigma) \tag{11}$$

as

$$E_H[\boldsymbol{\rho}] = \frac{1}{2}\int d^3r \int d^3r' \, \frac{e^2 n(\vec{r}) n(\vec{r'})}{4\pi\epsilon_0 |\vec{r}-\vec{r'}|} = \frac{1}{2}\sum_{\alpha,\beta,\gamma,\delta} U_{\alpha,\beta,\delta,\gamma}\rho_{\delta,\alpha}\rho_{\gamma,\beta}. \quad (12)$$

The exchange-correlation energy U_{xc} contains the complexity of the many particle problem. It is the electrostatic interaction of each electron with its exchange-correlation hole and the entropy term $-TS$. It should be noted that the exchange-correlation energy E_{xc} of DFT also contains a contribution from the kinetic energy, which is absent in the quantity U_{xc} used in rDMFT.

We restrict the present study to zero temperature and thus ignore the entropy term. To keep the notation simple, we suppress the index for the inverse temperature in the remainder of the text. Having laid down the basic concepts and our notation, we proceed with the concept of the hole function as a tool for the construction of approximate density-matrix functionals.

D. Hole function and the construction of density-matrix functionals

1. Hole function

In this section we discuss several exact properties of the hole function, which have been central to the development of density functionals, and in the following section we outline its role for the construction of approximate density-matrix functionals.

The hole function $h(\vec{r},\vec{r'})$ allows us to express the two-particle density $n^{(2)}(\vec{r},\vec{r'})$ in the form

$$n^{(2)}(\vec{r},\vec{r'}) = n(\vec{r})n(\vec{r'}) + n(\vec{r})h(\vec{r},\vec{r'}). \quad (13)$$

Note that the interaction-strength averaged hole function is used in DFT, while in rDMFT, the hole function at full interaction strength is of interest. The hole function integrates to minus one,

$$\int d^3r' \; h(\vec{r},\vec{r'}) = -1 \; , \quad (14)$$

and it is always negative [37].

These conditions constrain the shape of the hole function strongly, so that the exchange-correlation energy can be predicted reasonably well already with simple assumptions about the hole function. An insightful description of the hole function, which guided the development of a number of density-matrix functionals, has been given by Baerends and Buijse [38,39].

In the Hartree-Fock approximation, the hole function has the form

$$h(\vec{r},\vec{r'}) = \frac{-1}{n(\vec{r})}\sum_{m,n} f_m f_n \sum_{\sigma,\sigma'} \phi^*_m(\vec{x})\phi_n(\vec{x})\phi^*_n(\vec{x'})\phi_m(\vec{x'}). \quad (15)$$

As a consequence of the orthonormality of the natural orbitals, the sum rule Eq. (14) is obtained as

$$\int d^3r' \; h(\vec{r},\vec{r'}) = \frac{-1}{n(\vec{r})}\sum_{n\sigma} f_n^2 \phi^*_n(\vec{x})\phi_n(\vec{x}) = -1. \quad (16)$$

TABLE I. Dependence of the parameters $c_{m,n}$ on the occupations f_n as defined in Eq. (18) for density-matrix functionals used in this paper.

Hartree-Fock approximation	$c^{HF}_{m,n} = f_m f_n$
Müller functional [22]	$c^{M}_{m,n} = f_m^{\frac{1}{2}} f_n^{\frac{1}{2}}$
power functional [25]	$c^{P}_{m,n}(\alpha) = f_m^{\alpha} f_n^{\alpha}$

The sum rule is fulfilled exactly, when $f_n^2 = f_n$ that is for integer occupations. For fractional occupations, however, the Hartree-Fock expression violates the sum rule.

The exchange-correlation term in the Hartree-Fock approximation is

$$U^{HF}_{xc}[\boldsymbol{\rho}] = -\frac{1}{2}\sum_{m,n} f_m f_n \sum_{\alpha\beta\gamma\delta} U_{\alpha\beta,\delta\gamma} \times \langle\chi_\gamma|\phi_m\rangle\langle\phi_m|\chi_\alpha\rangle\langle\chi_\delta|\phi_n\rangle\langle\phi_n|\chi_\beta\rangle. \quad (17)$$

2. Construction of density-matrix functionals

Most empirical density-matrix functionals maintain this general form of the Hartree-Fock exchange term,

$$U_{xc}[\boldsymbol{\rho}] = -\frac{1}{2}\sum_{m,n} c_{m,n} \sum_{\alpha\beta\gamma\delta} U_{\alpha\beta,\delta\gamma} \times \langle\chi_\gamma|\phi_m\rangle\langle\phi_m|\chi_\alpha\rangle\langle\chi_\delta|\phi_n\rangle\langle\phi_n|\chi_\beta\rangle, \quad (18)$$

but replace the factor $f_n f_m$ in Eq. (17) by coefficients $c_{m,n}$ with a different dependence on the occupations.

Taking the hole function in the Hartree-Fock approximation Eq. (15) as a starting point, Müller [22] has shown that one can enforce the sum rule Eq. (14) also for fractional occupations with an ansatz

$$h(\vec{r},\vec{r'}) = \frac{1}{n(\vec{r})}\sum_{m,n} c^M_{n,m} \sum_{\sigma,\sigma'} \phi^*_m(\vec{x})\phi_n(\vec{x})\phi^*_n(\vec{x'})\phi_m(\vec{x'}) \quad (19)$$

with $c^M_{m,n} = \frac{1}{2}(f_m^{\frac{1}{2}+p} f_n^{\frac{1}{2}-p} + f_m^{\frac{1}{2}-p} f_n^{\frac{1}{2}+p})$.

Müller identified $p = 0$ as the choice that minimizes the violation of the positive definiteness of the hole function. This is the value used in nearly all applications.

Later, Sharma *et al.* [25] invented the so-called power functional by introducing an additional parameter α in the dependence of the coefficients $c_{m,n}$ on the occupations. They chose the form $c^P_{m,n}(\alpha) = f_m^{\alpha} f_n^{\alpha}$ that smoothly interpolates between the Müller functional with $\alpha = 1/2$ and the Hartree-Fock approximation with $\alpha = 1$. The main reason for this construction is according to Sharma *et al.* [25] the well known overcorrelating behavior of the Müller functional that will be mediated by a parameter $\alpha > 1/2$. The coefficients $c_{m,n}$ for the approximate density-matrix functionals considered in this paper are summarized in Table I.

III. HUBBARD DIMER

The two-site Hubbard model, the Hubbard dimer, is the simplest model for the covalent bond and bond breaking. The Hubbard dimer has a one-particle basis with four spin orbitals $|\chi_{1,\uparrow}\rangle, |\chi_{1,\downarrow}\rangle, |\chi_{2,\uparrow}\rangle, |\chi_{2,\downarrow}\rangle$, one for each site and spin. The only

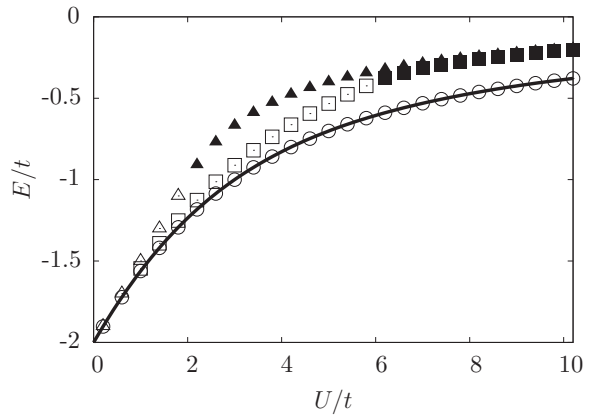

FIG. 1. Ground-state energy E of the half-filled Hubbard dimer as a function of interaction strength U/t for different density-matrix functionals. Circles: Müller functional. Squares: power functional with $\alpha = 0.53$. Triangles: Hartree-Fock approximation. Solid line: exact ground-state energy. The Müller functional produces the correct ground-state energy at half filling. Nonmagnetic states are indicated by open symbols and antiferromagnetic states by filled symbols.

nonzero matrix elements of the one-particle Hamiltonian

$$h_{\alpha,\beta} = -t(1 - \delta_{R_\alpha,R_\beta})\delta_{\sigma_\alpha,\sigma_\beta} \tag{20}$$

are those with orbitals having the same spin σ_α and σ_β but different centers R_α and R_β. All nonzero elements have the value $-t$, where t is positive. The orbital energies are chosen equal to zero.

Also the interaction tensor has a simple form, namely

$$U_{\alpha\beta,\gamma\delta} = \begin{cases} U & \text{if } \alpha = \gamma, \quad \beta = \delta \text{ and } R_\alpha = R_\beta \\ 0 & \text{otherwise} \end{cases}. \tag{21}$$

Thus, the Hamiltonian for the Hubbard dimer is

$$\hat{H} = -\sum_\sigma t(\hat{c}^\dagger_{1,\sigma}\hat{c}_{2,\sigma} + \hat{c}^\dagger_{2,\sigma}\hat{c}_{1,\sigma}) + \hat{W} \tag{22}$$

with the interaction

$$\hat{W} = \frac{1}{2}\sum_{i=1}^{2}\sum_{\sigma,\sigma'} U\hat{c}^\dagger_{i,\sigma}\hat{c}^\dagger_{i,\sigma'}\hat{c}_{i,\sigma'}\hat{c}_{i,\sigma}. \tag{23}$$

A. Total energy and density matrix

In Fig. 1, the total energy of the half-filled Hubbard dimer is shown as a function of interaction strength, along with the results obtained from approximate density-matrix functionals. Some of these data have been presented earlier [30]. Here, we emphasize the ground states obtained without biasing the magnetic configuration. We follow the convention commonly adopted in the solid state community of showing the graph for varying interaction strength U and fixed hopping t, so that the hopping sets the energy scale. Considering the bond dissociation problem, the natural choice would be to keep the interaction strength constant, while reducing the hopping parameter.

For the noninteracting case, i.e., at $U = 0$, the wave function is a Slater determinant of bonding states with opposite spin

$$|\Phi(U=0)\rangle = \tfrac{1}{2}(\hat{c}^\dagger_{1,\uparrow} + \hat{c}^\dagger_{2,\uparrow})(\hat{c}^\dagger_{1,\downarrow} + \hat{c}^\dagger_{2,\downarrow})|\mathcal{O}\rangle\,. \tag{24}$$

With $|\mathcal{O}\rangle$ we denote the vacuum state.

This wave function can be rewritten as a superposition of two eigenstates of the interaction operator

$$\begin{aligned}|\Phi(U=0)\rangle = {} & \tfrac{1}{2}(\hat{c}^\dagger_{1,\uparrow}\hat{c}^\dagger_{1,\downarrow} + \hat{c}^\dagger_{2,\uparrow}\hat{c}^\dagger_{2,\downarrow})|\mathcal{O}\rangle \\ & + \tfrac{1}{2}(\hat{c}^\dagger_{1,\uparrow}\hat{c}^\dagger_{2,\downarrow} - \hat{c}^\dagger_{1,\downarrow}\hat{c}^\dagger_{2,\uparrow})|\mathcal{O}\rangle. \end{aligned} \tag{25}$$

The first wave function contains contributions with two electrons on the same site, i.e., ionic states. Its interaction eigenvalue is U. The second wave function describes two electrons with opposite spin on different sites. Its interaction eigenvalue is zero.

The first term describes the double occupancy, that is the probability that two electrons are on the same site, which is penalized by the electron-electron interaction. The second term is attributed to left-right correlation, as it describes the probability that the two electrons are on different sites.

As the interaction strength is increased, the contribution of the first wave function, being responsible for double occupancy, is suppressed. The wave function obtains the form

$$\begin{aligned}|\Phi(\vartheta)\rangle = {} & \frac{1}{\sqrt{2}}(\hat{c}^\dagger_{1,\uparrow}\hat{c}^\dagger_{1,\downarrow} + \hat{c}^\dagger_{2,\uparrow}\hat{c}^\dagger_{2,\downarrow})|\mathcal{O}\rangle\cos\left(\vartheta + \frac{\pi}{4}\right) \\ & + \frac{1}{\sqrt{2}}(\hat{c}^\dagger_{1,\uparrow}\hat{c}^\dagger_{2,\downarrow} - \hat{c}^\dagger_{1,\downarrow}\hat{c}^\dagger_{2,\uparrow})|\mathcal{O}\rangle\sin\left(\vartheta + \frac{\pi}{4}\right). \end{aligned} \tag{26}$$

With a basis set in the order $(|\chi_{1,\uparrow}\rangle, |\chi_{1,\downarrow}\rangle, |\chi_{2,\uparrow}\rangle, |\chi_{2,\downarrow}\rangle)$, the one-particle reduced density matrix has the form

$$\rho_{\alpha,\beta}(\vartheta) = \frac{1}{2}\begin{pmatrix} 1 & 0 & \cos(2\vartheta) & 0 \\ 0 & 1 & 0 & \cos(2\vartheta) \\ \cos(2\vartheta) & 0 & 1 & 0 \\ 0 & \cos(2\vartheta) & 0 & 1 \end{pmatrix}. \tag{27}$$

The interaction energy is proportional to the double occupancy

$$\langle\Phi(\vartheta)|\hat{W}|\Phi(\vartheta)\rangle = U\cos^2\left(\vartheta + \frac{\pi}{4}\right) \tag{28}$$

and the noninteracting energy is

$$\langle\Phi(\vartheta)|\hat{h}|\Phi(\vartheta)\rangle = -2t\cos(2\vartheta). \tag{29}$$

The value of ϑ results from an equilibrium between the forces from the interaction energy Eq. (28) and those from the one-particle energy Eq. (29), which determines $\vartheta(U)$ as

$$\vartheta(U) = \arctan\left(\sqrt{1 + \left(\frac{U}{4t}\right)^2} + \frac{U}{4t}\right) - \frac{\pi}{4}. \tag{30}$$

The value $\vartheta(U)$ varies from zero to $\pi/4$ with increasing interaction strength.

The resulting optimum energy has the form

$$E = -2t\left[\sqrt{1 + \left(\frac{U}{4t}\right)^2} - \frac{U}{4t}\right]. \tag{31}$$

As the interaction increases, the wave function changes continuously from a Slater determinant of bonding states Eq. (25) at $U = 0$ to a singlet state with antiferromagnetic correlations.

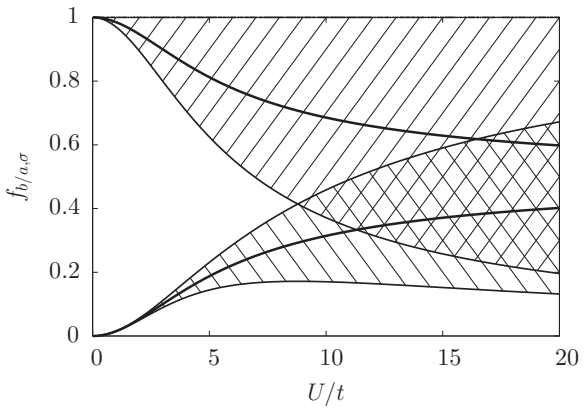

FIG. 2. Occupations $f_{b,\sigma}$ and $f_{a,\sigma}$ from Eq. (48) of the half-filled dimer obtained with the Müller functional as a function of interaction strength U/t. The striped regions indicate the range of occupations in the manifold of degenerate ground states. The thick solid lines indicate the mean values for the pair of occupations in the corresponding striped region. It also represents the degenerate occupations for the nonmagnetic solution of the Müller functional. The occupations of the nonmagnetic solution of the Müller functional coincide with those of the exact ground state of the Hubbard dimer.

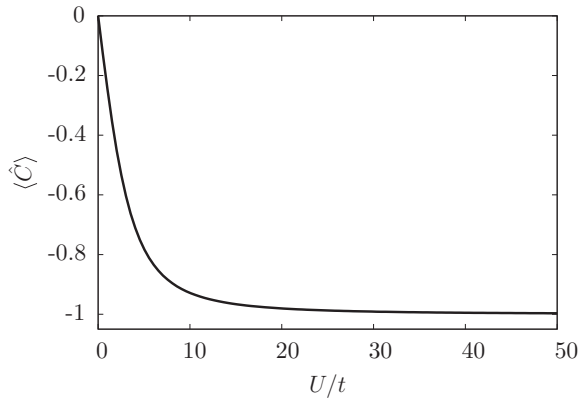

FIG. 3. Site correlation $\langle\hat{C}\rangle$ as defined in Eq. (34) of the half-filled Hubbard dimer as a function of U/t. With increasing interaction strength U/t the site correlation shows the transition from delocalized electrons $\langle\hat{C}\rangle = 0$ to the left-right correlated state with $\langle\hat{C}\rangle = -1$.

During this process, the bond strength is weakened and the covalent bond vanishes completely in the limit of infinite interaction. This loss of covalent bonding can also be described as localization of electrons on opposite sites, which raises the kinetic energy as a consequence of Heisenberg's uncertainty principle.

What has been described here is what is called static correlation [5]: The states for finite interaction can no more be described by a single Slater determinant, but four Slater determinants are required.

B. Natural orbitals and occupations

Interestingly, the natural orbitals do not depend on the interaction strength U. They are the bonding and antibonding states

$$\begin{aligned} |b,\sigma\rangle &:= \frac{1}{\sqrt{2}}(|\chi_{1,\sigma}\rangle + |\chi_{2,\sigma}\rangle) \\ |a,\sigma\rangle &:= \frac{1}{\sqrt{2}}(|\chi_{1,\sigma}\rangle - |\chi_{2,\sigma}\rangle). \end{aligned} \tag{32}$$

Both orbitals are spread over both atoms, and the natural orbitals are identical to those of the noninteracting system.

The loss of bonding is, however, expressed by the fact that the occupations become fractional. The occupations are shown in Fig. 2. Their exact values $f_{b,\sigma}$ for the bonding states and $f_{a,\sigma}$ for the antibonding states are

$$\begin{aligned} f_{b,\sigma} &= \tfrac{1}{2} + \tfrac{1}{2}\cos(2\vartheta) \\ f_{a,\sigma} &= \tfrac{1}{2} - \tfrac{1}{2}\cos(2\vartheta). \end{aligned} \tag{33}$$

In the noninteracting case, the occupations are integer, with filled bonding states and unoccupied antibonding states. In the limit of large interaction strength the occupations approach $1/2$ for all four natural orbitals. In this limiting case with equally occupied bonding and antibonding states, the net bond strength vanishes completely. In the context of natural orbitals, we describe the effect as quantum fluctuations that create electron-hole pairs. These electron-hole pairs destroy the covalent bond with increasing interaction.

C. Correlations

In view of the following discussion, it is instructive to investigate the correlations of the electrons. The probability for an electron to be on one site and the other on the other site, we name it "site correlation," is given by the expectation value of

$$\hat{C} = (\hat{c}^\dagger_{2,\uparrow}\hat{c}_{2,\uparrow} - \hat{c}^\dagger_{1,\uparrow}\hat{c}_{1,\uparrow})(\hat{c}^\dagger_{2,\downarrow}\hat{c}_{2,\downarrow} - \hat{c}^\dagger_{1,\downarrow}\hat{c}_{1,\downarrow}). \tag{34}$$

For a state where both electrons bunch on one site, the expectation value of this operator is one, while if they localize on opposite sites, the expectation value is minus one. If it is zero, then the electrons are delocalized, i.e., there is no correlation between the positions of both electrons. The correlation operator $\hat{C}$ is a two-particle operator and is not accessible from the one-particle density matrix. The exact solution for the correlation expectation value for the ground state is given by

$$\langle\hat{C}\rangle = -\sin(2\vartheta(U)), \tag{35}$$

where $\vartheta(U)$ is given by Eq. (30). We can see in Fig. 3 that the site correlation vanishes without interaction, while the electrons antibunch for strong correlation so that $\langle\hat{C}\rangle$ approaches minus one. A site correlation of minus one indicates that each electron is fully localized either at one or at the other site, while the other is always at the other site. This is the basic notion of left-right correlation.

Of interest will also be the magnetic nature of the wave functions. The operator for the spin on site i is

$$\hat{\vec{S}}_i = \frac{\hbar}{2}\begin{pmatrix} \hat{c}^\dagger_{i,\uparrow}\hat{c}_{i,\downarrow} + \hat{c}^\dagger_{i,\downarrow}\hat{c}_{i,\uparrow} \\ -i\hat{c}^\dagger_{i,\uparrow}\hat{c}_{i,\downarrow} + i\hat{c}^\dagger_{i,\downarrow}\hat{c}_{i,\uparrow} \\ \hat{c}^\dagger_{i,\uparrow}\hat{c}_{i,\uparrow} - \hat{c}^\dagger_{i,\downarrow}\hat{c}_{i,\downarrow} \end{pmatrix}. \tag{36}$$

For the wave function in Eq. (26), the total spin expectation value $\langle(\hat{\vec{S}}_1 + \hat{\vec{S}}_2)^2\rangle$ vanishes, and consequently the spin

expectation value $\langle\hat{\vec{S}}_i\rangle$ on each site vanishes as well. Nevertheless, the spins on different sites are antiferromagnetically correlated, that is

$$\langle\Phi(\vartheta)|\hat{\vec{S}}_1\cdot\hat{\vec{S}}_2|\Phi(\vartheta)\rangle=-\tfrac{3}{8}\hbar^2[1+\sin(2\vartheta)]\leqslant 0. \quad (37)$$

An antiferromagnetic correlation is already present in the noninteracting state, which expresses the nonvanishing contribution of the left-right correlated states to the Slater determinant built from bonding orbitals. As the interaction increases the left-right correlation doubles, which reflects in the increase of the antiferromagnetic correlation expressed in Eq. (37).

IV. METHODS

The natural orbitals and occupations have been optimized in the Car-Parrinello spirit [40] using a fictitious Lagrangian of the form

$$\begin{aligned}\mathcal{L}=&\frac{1}{2}\sum_n m_f\dot{x}_n^2+\sum_n f(x_n)m_\psi\sum_\alpha|\dot{a}_{\alpha,n}|^2\\&-\sum_n f(x_n)\sum_{\alpha,\beta}a_{\alpha,n}h_{\beta,\alpha}a^*_{\beta,n}-F^{\hat{W}}\left[\sum_n a_{\alpha,n}f(x_n)a^*_{\beta,n}\right]\\&+\sum_{n,m}\Lambda_{m,n}\left(\sum_\alpha a^*_{\alpha,n}a_{\alpha,m}-\delta_{n,m}\right)\\&+\mu\left(\sum_n f(x_n)-N\right).\end{aligned} \quad (38)$$

The natural orbitals are given by the complex-valued coefficients $a_{\alpha,n}=\langle\chi_\alpha|\phi_n\rangle$ as

$$|\phi_n\rangle=\sum_\alpha|\chi_\alpha\rangle a_{\alpha,n} \quad (39)$$

and the occupations $f_n=f(x_n)$ are expressed by the real-valued dynamical variables x_n with $f(x)=[1-\cos(x)]/2$. The orthonormality of the natural orbitals is enforced with the Lagrange multipliers $\Lambda_{m,n}$, which form a hermitian matrix, and the particle number is constrained with the chemical potential μ.

In order to avoid any bias in our results, the wave functions and occupations are initialized as random numbers between zero and one. Then the constraints, i.e., orthonormality of the natural orbitals and total particle number, are imposed. For the actual minimization, the Euler-Lagrange equations for the occupation variables x_n and the coefficients $a_{\alpha,n}$ are propagated using the Verlet algorithm under the additional action of a friction term. The constraints are enforced with the help of Lagrange multipliers [41]. The friction term leads to energy dissipation and monotonic decrease of the total energy until the ground state or a metastable state is reached. The phase space has been explored by repeating the calculation, in order to identify the global minimum and potential degenerate ground states.

An analytical form of the natural orbitals has been extracted by inspection of the results obtained numerically. The resulting ansatz for the natural orbitals has been verified by optimizing the total energy in this subspace and comparing the energies. While the numerical formulation is invariant under global spin rotations, spatial reflection, or application of a phase factor, the analytical results are given for a particular choice.

V. PERFORMANCE OF DENSITY-MATRIX FUNCTIONALS

A. Hartree-Fock approximation

After having covered the main properties of the exact ground state of the half-filled Hubbard dimer in Sec. III, we turn now to the results obtained from approximate density-matrix functionals. We begin with the Hartree-Fock approximation given in Eq. (17), which has been the starting point for the development of other density-matrix functionals investigated in this study as discussed in Sec. II D 2.

1. Nonmagnetic solution

If one constrains the density matrix to remain nonmagnetic, the natural orbitals do not depend on the interaction strength. The corresponding total energy has the form

$$E^{HF}(U)=-2t+\frac{U}{2}. \quad (40)$$

The energy Eq. (40) for the Hubbard dimer with two infinitely separated atoms, that is in the limit of $t\to 0$, results in a nonzero energy $U/2$, while the correct energy vanishes, because each isolated atom has a single electron that does not interact with itself. This reflects the well known difficulty of restricted, i.e., non-spin-polarized, Hartree-Fock to describe the dissociation of chemical bonds.

While the errors caused by non-spin-polarized Hartree-Fock calculations are severe, they are not our main concern. Today's electronic structure calculations should consider a spin polarization whenever a magnetization provides a lower energy. Allowing for spin polarization, i.e., as in unrestricted Hartree-Fock or spin-density functional theory, improves the description dramatically. Nevertheless, the transition from the weakly correlated to the strongly correlated regime still differs in many ways from the correct behavior. These differences are of interest in the following discussion.

2. Antiferromagnetic solution

If one allows for general variations of the density matrix, there is a crossover at $U=2t$ from a nonmagnetic solution at small interactions to an antiferromagnetic solution at large interactions.

One set of natural orbitals that describes the transition to the antiferromagnetic solution beyond $U=2t$ has the form

$$\begin{aligned}\left|\phi_1^{HF}(\gamma)\right\rangle&=+|b,\uparrow\rangle\cos(\gamma)+|a,\uparrow\rangle\sin(\gamma)\\\left|\phi_2^{HF}(\gamma)\right\rangle&=+|b,\downarrow\rangle\cos(\gamma)-|a,\downarrow\rangle\sin(\gamma)\\\left|\phi_3^{HF}(\gamma)\right\rangle&=-|b,\uparrow\rangle\sin(\gamma)+|a,\uparrow\rangle\cos(\gamma)\\\left|\phi_4^{HF}(\gamma)\right\rangle&=+|b,\downarrow\rangle\sin(\gamma)+|a,\downarrow\rangle\cos(\gamma).\end{aligned} \quad (41)$$

The first two natural orbitals are occupied and the remaining two are unoccupied.

The corresponding many-particle wave function,

$$|\Phi^{HF}(\gamma)\rangle = \left[\hat{c}^{\dagger}_{1,\uparrow}\cos\left(\gamma-\frac{\pi}{4}\right)+\hat{c}^{\dagger}_{2,\uparrow}\cos\left(\gamma+\frac{\pi}{4}\right)\right]\left[\hat{c}^{\dagger}_{1,\downarrow}\cos\left(\gamma+\frac{\pi}{4}\right)-\hat{c}^{\dagger}_{2,\downarrow}\cos\left(\gamma-\frac{\pi}{4}\right)\right]|\mathcal{O}\rangle, \tag{42}$$

is a single Slater determinant in the basis of the natural orbitals. For $\gamma = 0$, we recover the ground state of the noninteracting limit given in Eq. (24).

The many-particle wave function Eq. (42) has the one-particle reduced density matrix in the basis $(|\chi_{1,\uparrow}\rangle,|\chi_{1,\downarrow}\rangle,|\chi_{2,\uparrow}\rangle,|\chi_{2,\downarrow}\rangle)$

$$\rho^{HF}(\gamma) = \frac{1}{2}\begin{pmatrix} 1+\sin(2\gamma) & 0 & \cos(2\gamma) & 0 \\ 0 & 1-\sin(2\gamma) & 0 & \cos(2\gamma) \\ \cos(2\gamma) & 0 & 1-\sin(2\gamma) & 0 \\ 0 & \cos(2\gamma) & 0 & 1+\sin(2\gamma) \end{pmatrix}. \tag{43}$$

The interaction energy is

$$\langle\Phi^{HF}(\gamma)|\hat{W}|\Phi^{HF}(\gamma)\rangle = \tfrac{1}{2}U\cos^2(2\gamma) \tag{44}$$

and the noninteracting energy is given by

$$\langle\Phi^{HF}(\gamma)|\hat{h}|\Phi^{HF}(\gamma)\rangle = -2t\cos(2\gamma)\,. \tag{45}$$

Increasing the parameter γ in the wave function from 0, i.e., the noninteracting limit, allows one to trade part of the covalent bond, i.e., the kinetic energy, for a reduction of the interaction energy.

The total energy is minimized by

$$\gamma(U) = \begin{cases} 0 & \text{for } U \leqslant 2t \\ \frac{1}{2}\arccos\left(\frac{2t}{U}\right) & \text{for } U > 2t. \end{cases} \tag{46}$$

For $U \leqslant 2t$, the system remains nonmagnetic and the natural orbitals are given by bonding and antibonding orbitals as in the case of nonmagnetic dimer. But for $U > 2t$, the system becomes an antiferromagnet, whereas the exact many-particle wave function is a singlet with antiferromagnetic correlations. The antiferromagnetic state is a superposition of a singlet and a triplet wave function and thus it is not an eigenstate of $\hat{S}^2$. We can paraphrase it as a violation of rotational symmetry in the spin degrees of freedom, i.e., of SU(2) spin symmetry.

B. Müller functional

Müller's approximation to the density-matrix functional introduced in Sec. II D 2 leads to the exact ground-state energy for the half-filled Hubbard dimer for all interaction strengths [30,42]. In contrast to the Hartree-Fock approximation, there is no unphysical transition to an antiferromagnetic state.

1. Magnetic solutions

Even though the Müller functional produces exact ground-state energies for the half-filled Hubbard dimer, we also detected a major flaw, namely that there is a one-dimensional manifold of magnetic states which are degenerate to the correct nonmagnetic solution. The infinite magnetic susceptibility obtained with the Müller functional is in contrast to the exact behavior: At zero temperature and finite interaction strength, the true magnetic susceptibility vanishes because of the finite singlet-triplet splitting [43,44].

Our unbiased optimizations using the Müller functional result in natural orbitals equivalent to the exact ones given in Eq. (32), namely the bonding and antibonding orbitals.

With the natural orbitals of Eq. (32), the total energy for the half-filled dimer obtained from the Müller functional can be expressed solely by the occupations as

$$E^M = -2t + \frac{1}{2}U + 2t\left(\sum_{\sigma} f_{a\sigma}\right) - \frac{1}{2}U\sum_{\sigma}\sqrt{f_{a\sigma}\,f_{b\sigma}}. \tag{47}$$

The first two terms, which are independent of the occupations, are identical to the total energy Eq. (40) of the spin-restricted Hartree-Fock approximation. If only the bonding states are occupied, the remaining terms of Eq. (47) vanish and the Müller functional gives the same result as the Hartree-Fock approximation.

The occupations are obtained as the minimum of Eq. (47) for occupations between zero and one that add up to the total particle number of $N = 2$. For a given interaction strength, we find that the minimum condition does not define a single point, but a line of degenerate states parameterized by the parameter s

$$\begin{aligned} f^M_{a,\uparrow}(s) &= \frac{1}{1+R^2} + s, \\ f^M_{a,\downarrow}(s) &= \frac{1}{1+R^2} - s, \\ f^M_{b,\uparrow}(s) &= R^2\left(\frac{1}{1+R^2} + s\right), \\ f^M_{b,\downarrow}(s) &= R^2\left(\frac{1}{1+R^2} - s\right), \end{aligned} \tag{48}$$

where $R = 4t/U + \sqrt{1+(4t/U)^2}$.

The requirement, that the occupations remain between zero and one, limits the parameter s to the interval

$$s \in \left[-\frac{1}{R^2(1+R^2)}, \frac{1}{R^2(1+R^2)}\right]. \tag{49}$$

The range of the occupations, which minimize the total energy Eq. (47), is shown in Fig. 2 as a function of interaction strength U/t. In the limit of infinite interaction strengths, we have $R = 1$, respectively, $s \in [-1/2, 1/2]$ and the possible occupations $f^M_{a/b,\sigma}(s) = 1/2 + \sigma s$ cover the whole range from zero to one.

All solutions, except the physical one with equally occupied bonding states and equally occupied antibonding states, have a magnetic moment. Hence, the magnetic susceptibility

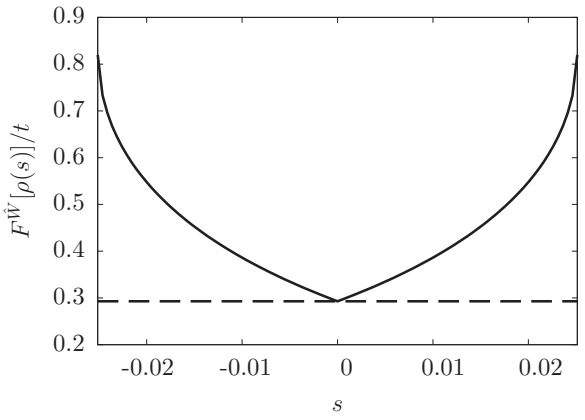

FIG. 4. Müller density-matrix functional (dashed line) and the exact functional (solid line) as a function of the line parameter s for $U = 4t$. The density matrix $\rho(s)$ is given by Eq. (32) and Eq. (48). The values of the exact functional have been obtained by a constrained search over an ensemble of many-particle wave functions. The point $s = 0$, where the Müller functional and the exact functional coincide, corresponds to the symmetric solution ($m_z = 0$).

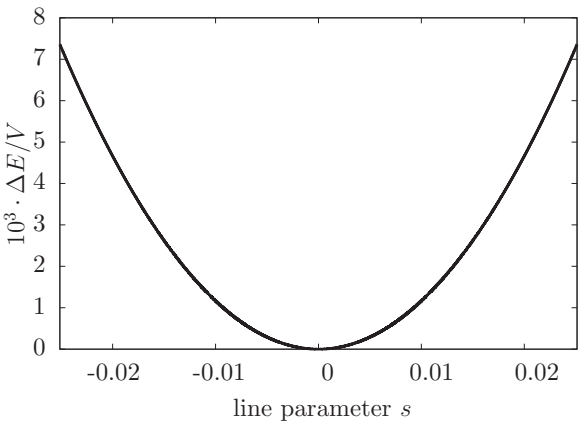

FIG. 5. Energy $\Delta E = E[V,s] - E[V,s = 0]$ of Eq. (52) of the Hubbard dimer obtained with the Müller functional including an offsite interaction in first-order perturbation theory with $U = 4t$ along the manifold Eq. (48) of ground states. The point $s = 0$ indicates the nonmagnetic solution.

predicted by the Müller functional is infinite for all finite interaction strengths.

The magnetization of each site in the ground state of the Müller functional obtained with the occupations given by Eq. (48) has the form

$$\begin{aligned} m^z(s) &= \tfrac{1}{2}\left[f^M_{b,\uparrow}(s) - f^M_{b,\downarrow}(s) + f^M_{a,\uparrow}(s) - f^M_{a,\downarrow}(s)\right]\mu_B \\ &= (1+R^2)s\;\mu_B \end{aligned} \tag{50}$$

with the Bohr magneton μ_B. It can assume any value with $|m_z| < 1/R^2\;\mu_B$.

In Fig. 4, the density-matrix functional of Müller is compared to the exact density-matrix functional in the range of degenerate ground states of the Müller functional. The exact density-matrix functional is obtained from a constrained search over an ensemble of fermionic many-particle wave functions [19] for density matrices parametrized by Eq. (32) and Eq. (48). The enormous difference in the functionals illustrates the severe problems of the Müller functional to describe the magnetic structure properly and indicates a systematic flaw in the functional.

2. *Offsite interaction*

The finding of an infinite magnetic susceptibility raises the question whether this finding transfers to more realistic systems. One of the major restrictions of the Hubbard model is the limitation to pure on-site interactions. Therefore, we extended the Hubbard model to include also an electron-electron interaction V between the sites

$$\begin{aligned} \hat{W} = &\frac{1}{2}\sum_i \sum_{\sigma,\sigma'} U \hat{c}^\dagger_{i,\sigma}\hat{c}^\dagger_{i,\sigma'}\hat{c}_{i,\sigma'}\hat{c}_{i,\sigma} \\ &+ \frac{1}{2}\sum_{i\neq j}\sum_{\sigma} V \hat{c}^\dagger_{i,\sigma}\hat{c}^\dagger_{j,\sigma}\hat{c}_{i,\sigma}\hat{c}_{j,\sigma}\,. \end{aligned} \tag{51}$$

Using the density matrices from the degenerate manifold of ground states without offsite interaction, i.e., with bonding and antibonding states as natural orbitals Eq. (32) and the occupations from Eq. (48), the effect of the offsite interaction has been explored up to first order in the offsite interaction V. This leads to

$$\begin{aligned} E^M[V,s] = E^M[0,s] + \frac{V(R^2-1)^2}{2} \\ \times\left[\left(\frac{2}{1+R^2}\right)^2 + s^2\right] + \mathcal{O}(V^2). \end{aligned} \tag{52}$$

$E^M[0,s]$ is the s-independent total energy obtained with the Müller functional for the Hubbard dimer in the absence of an offsite interaction. It is given by Eqs. (47) and (48).

As shown in Fig. 5, the offsite term lifts the degeneracy of the ground states of the Müller functional. The nonmagnetic solution with $s = 0$ is now favored. This indicates that this artificial degeneracy may not be immediately apparent in real systems.

Nevertheless, as evident from the comparison with the exact functional shown in Fig. (4), the changes produced by the offsite term are far too small: In order to produce an energy difference between the maximally polarized state [see Eq. (49)] and the unpolarized state comparable to the exact result shown in Fig. 4, an unrealistically large offsite interaction parameter of order $V = 10t$ would be required.

C. Power functional

After having investigated the Hartree-Fock approximation and the Müller functional, we consider now the power functional invented by Sharma *et al.* [25], which we described in Sec. II D 2.

The occupations of the Hubbard dimer obtained from the power functional are shown in Fig. 6 for a value $\alpha = 0.53$. Whereas the density-matrix functional in the Hartree-Fock approximation produces integer and pairwise identical occupations, the power functional produces fractional occupations which are not identical in pairs.

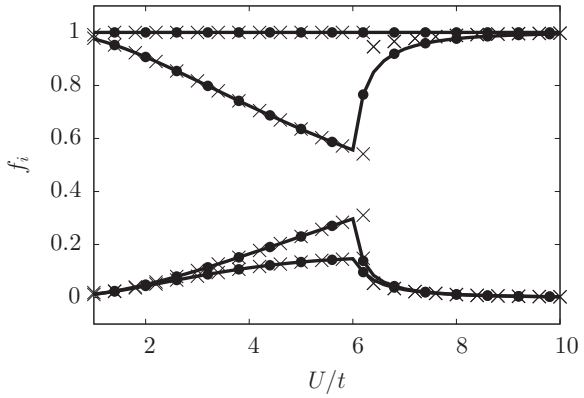

FIG. 6. Occupations f_i as a function of U/t for the power functional with $\alpha = 0.53$. Solid dots have been obtained from an unbiased optimization of the power functional. The solid lines are obtained from a restricted optimization using the noncollinear natural orbitals of the ansatz Eq. (56). The diagonal crosses are obtained from a restricted optimization using the collinear natural orbitals Eq. (55) of the Hartree-Fock approximation.

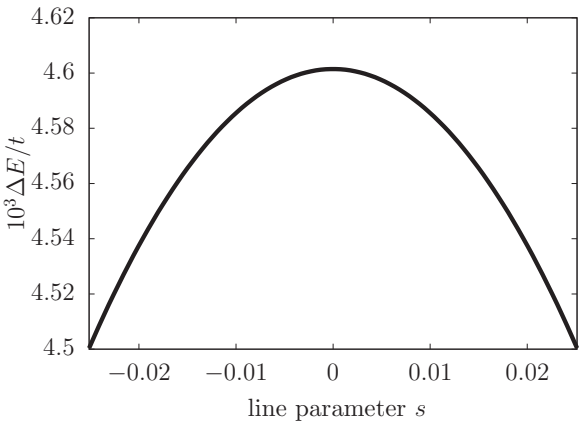

FIG. 7. Total energy difference $\Delta E = E^P_{\alpha=1/2+\epsilon}[\rho(s)] - E^P_{\alpha=1/2}[\rho(s)]$ given by Eq. (53) for $U = 4t$ using the power functional approximation with $\epsilon = 10^{-3}$ as a function of the line parameter s that parametrizes the one-particle reduced density matrix according to Eq. (48).

Near $U = 6t$, we observe a transition. This transition separates the Müller-like behavior at small interactions from a Hartree-Fock-like behavior at large interactions.

(1) At small interactions, the solutions are analogous to those of the Müller functional. However, from the manifold of degenerate ground states of the Müller functional, the power functional favors the state with maximal ferromagnetic moments.

(2) At larger interactions, the ground state undergoes a transition into a noncollinear ground state. For very large interaction the state approaches the Hartree-Fock-like antiferromagnetic state.

1. Ferromagnetic solution in the weakly interacting regime:

The occupations in the weakly interacting regime can be understood as follows: In case of the Müller density-matrix functional, we have shown in Sec. V B that there exists a manifold of degenerate ground-state density matrices on the line given by Eq. (48). If we increase the parameter α of the power functional infinitesimally as $\alpha = \frac{1}{2} + \epsilon$ where $\epsilon > 0$, and restrict ourselves to interaction strengths U/t where the natural orbitals are bonding and antibonding states, Eq. (32), the total energy along the line given by Eq. (48) is

$$E^P_{\alpha=\frac{1}{2}+\epsilon}(s) = 2t\left(\frac{2}{1+R^2} - 1\right) + U - \frac{U}{4}\sum_{\sigma=\pm 1}(1+R^{1+2\epsilon})^2\left(\frac{1}{1+R^2} + \sigma s\right)^{1+2\epsilon}, \tag{53}$$

where $R = 4t/U + \sqrt{1+(4t/U)^2}$. The energy in Eq. (53), shown in Fig. 7, has a negative curvature along the line parameter s and the minima lie at the boundaries given in Eq. (49).

At these boundaries, the extreme nonsymmetric solutions of the Müller functional, one of the states is always fully occupied (see Fig. 2) because this maximum occupation limits the range of degenerate solutions. This explains the corresponding observation in Fig. 6.

Unfortunately, any change of the parameter α away from the value of the Müller functional, destroys the nonmagnetic ground state in favor of an unphysical ferromagnetic state.

2. Large-interaction regime

The Hartree-Fock approximation exhibits a transition from a nonmagnetic state to an antiferromagnetic state at $U = 2t$. This transition is absent in the Müller functional, but it is present in the power functional for all other values of $\alpha > \frac{1}{2}$.

In order to explore how the power functional interpolates between these two extreme cases, we calculated the product $\langle \hat{\vec{S}}_1 \rangle \cdot \langle \hat{\vec{S}}_2 \rangle$ of the spin expectation values at the two sites of the dimer. A positive value of $\langle \hat{\vec{S}}_1 \rangle \cdot \langle \hat{\vec{S}}_2 \rangle$ corresponds to a ferromagnetic, a negative value to an antiferromagnetic spin alignment. The maximum absolute value is $\hbar^2/4$.

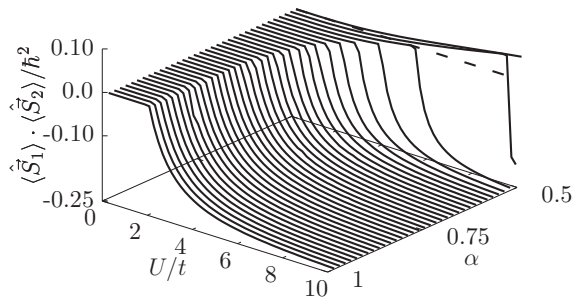

FIG. 8. Scalar product $\langle \hat{\vec{S}}_1 \rangle \cdot \langle \hat{\vec{S}}_2 \rangle$ of the spin expectation vectors on the two sites of the Hubbard dimer as an indicator for the transition to the antiferromagnetic state within the power functional approximation with the parameter α for the Hubbard dimer at various interaction strengths. A positive value indicates a ferromagnetic state, a negative value an antiferromagnetic state. For the Müller functional, i.e., $\alpha = 1/2$, the dashed line represents the result for the symmetric solutions and the solid line the corresponding degenerate result for the degenerate maximally polarized state.

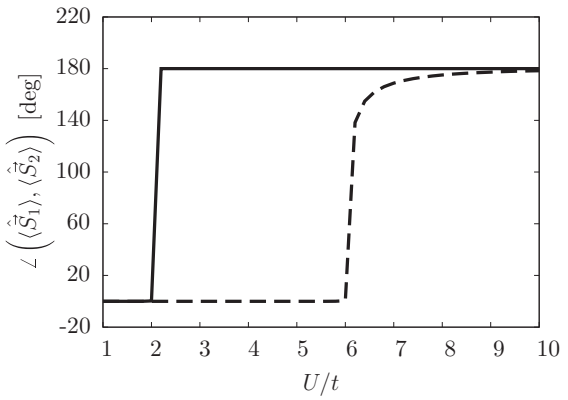

FIG. 9. Angle between the spin expectation vectors $\langle\vec{S}_1\rangle$ and $\langle\vec{S}_2\rangle$ on the two sites of the Hubbard dimer as function of the interaction strength U. Dashed line: power functional with the parameter $\alpha = 0.53$; solid line: Hartree-Fock approximation. This angle is a measure of collinearity of natural orbitals.

For the Hubbard dimer at half filling, $\langle\hat{\vec{S}}_1\rangle \cdot \langle\hat{\vec{S}}_2\rangle$ is shown in Fig. 8 as a function of interaction strength U/t and the parameter α of the power functional. For the Müller functional discussed in Sec. V B 1, i.e., for $\alpha = 1/2$, we consider the solution with the strongest polarization, because this is the state that continuously matches to the solutions of the power functional. In this ferromagnetic state, $\langle\hat{\vec{S}}_1\rangle \cdot \langle\hat{\vec{S}}_2\rangle$ is positive. Unfortunately, the correct nonmagnetic state is not a ground state of the power functional for $\alpha > \frac{1}{2}$.

At a critical interaction strength $U_c(\alpha)$ the power functional exhibits a transition from this ferromagnetic state into a complex noncollinear state with a mostly antiferromagnetic spin alignment. The angle between the magnetization on the two sites is shown in Fig. 9.

Figure 8 clearly shows the location of the transition between the ferromagnetic and the antiferromagnetic noncollinear regime. The critical interaction strength $U_c(\alpha)$ of this transition is infinite for the Müller functional. As the parameter α is increased, the critical interaction strength falls off rapidly and approaches the value $U_c(\alpha = 1) = 2t$ of the Hartree-Fock approximation.

Thus, the power functional exhibits a Hartree-Fock-like transition into an antiferromagnetic ground state except for the limiting case, the Müller functional. By choosing the parameter α sufficiently close to $1/2$, the transition can be shifted into a regime that is physically less important.

a. Collinear approximation using the Hartree-Fock natural orbitals. In order to get a qualitative understanding of the asymmetric occupations (Ref. Fig. 6) and the critical value of interaction strength U_c of the transition to antiferromagnetic solutions (Ref. Fig. 8), we use an ansatz that covers both extreme cases, namely the Müller functional with $\alpha = \frac{1}{2}$ and the Hartree-Fock approximation with $\alpha = 1$. These are, one the one hand, the asymmetric natural orbitals Eq. (41) that can describe the antiferromagnetic state of the Hartree-Fock approximation. On the other hand, the ansatz allows for fractional occupations to capture the nature of the ground state of the Müller functional.

With this ansatz, the one-particle reduced density matrix $\rho(f_1, \ldots, f_4, \gamma)$ is a function of occupations f_n and the angle γ and the corresponding total energy $E^{P,\alpha}$ obtained with the power functional is

$$E^P_\alpha[\rho(f_1,\ldots,f_4,\gamma)] = E^{\text{kin}}[\rho(f_1,\ldots,f_4,\gamma)] + F^P_\alpha[\rho(f_1,\ldots,f_4,\gamma)] \tag{54}$$

where

$$\begin{aligned} E^{\text{kin}}[\rho(f_1,\ldots,f_4,\gamma)] &= -t\cos(2\gamma)(f_1+f_2-f_3-f_4) \\ F^P_\alpha[\rho(f_1,\ldots,f_4,\gamma)] &= \frac{U}{4}\left[(f_1+f_2+f_3+f_4)^2 - \left(f_1^\alpha + f_3^\alpha\right)^2 - \left(f_2^\alpha + f_4^\alpha\right)^2\right] \\ &\quad + \frac{U}{4}\sin^2(2\gamma)\left[(f_2+f_3-f_4-f_1)^2 - \left(f_1^\alpha - f_3^\alpha\right)^2 - \left(f_2^\alpha - f_4^\alpha\right)^2\right]. \end{aligned} \tag{55}$$

An approximation, which is a strict upper bound, for the total energy of the power functional is obtained by minimizing Eq. (55) for a half-filled system with occupations between zero and one.

As a characteristic example, the resulting occupations for $\alpha = 0.53$ are shown in Fig. 6. The properties of this ansatz with regard to the description of the transition to the antiferromagnetic state will be investigated in the following section after a more general discussion of the transition.

The ansatz using the collinear natural orbitals Eq. (41) and arbitrary occupations is, however, not able to describe the true ground state for the power functional in the strongly interacting regime. The energy difference of the ansatz to the unbiased solution is shown in Fig. 10. The deviation is largest near the transition. The transition point is slightly displaced by the collinear ansatz, which explains the sharp rise. For larger interactions, the error due to the collinear approximation falls off rapidly. It should be noted that the overall error due to the restricted ansatz is apparently small. For the parameter $\alpha = 0.53$ used in Eq. (10), the maximum error in the energy is less than 1% of the binding energy.

b. Beyond the collinear approximation. The ansatz using the Hartree-Fock natural orbitals already gives a fairly good description of the ground state of the power functional. How do the natural orbitals of the power functional differ from those of the Hartree-Fock solution?

In the large interaction region, the power functional produces noncollinear ground states. The natural orbitals of the power functional can be represented as superpositions of

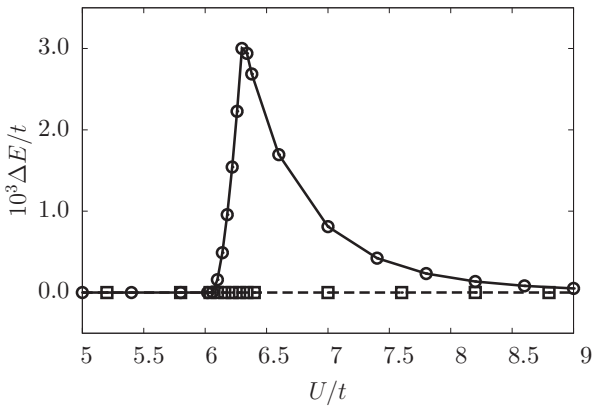

FIG. 10. Energy difference ΔE of the power functional with $\alpha = 0.53$ between the density matrices obtained by a constrained and an unbiased optimization. ΔE obtained from constrained optimization with the natural orbitals from the Hartree-Fock approximation in Eq. (41) is the solid line with circle symbols, while the ΔE obtained from constrained optimization with the noncollinear natural orbitals of Eq. (56) is the dashed line with square symbols.

bonding and antibonding states,

$$\begin{aligned}
\left|\phi_1^P\right\rangle &= |b,\uparrow\rangle \cos(\beta_1) - |a,\downarrow\rangle \sin(\beta_1) \\
\left|\phi_2^P\right\rangle &= |b,\downarrow\rangle \cos(\beta_2) - |a,\uparrow\rangle \sin(\beta_2) \\
\left|\phi_3^P\right\rangle &= |b,\uparrow\rangle \sin(\beta_1) + |a,\downarrow\rangle \cos(\beta_1) \\
\left|\phi_4^P\right\rangle &= |b,\downarrow\rangle \sin(\beta_2) + |a,\uparrow\rangle \cos(\beta_2)\,.
\end{aligned} \tag{56}$$

The two angles β_1 and β_2 are free variational parameters. The natural orbitals of the noninteracting system, respectively, those of the Müller functional, are obtained with $\beta_1 = \beta_2 = 0$. The values of the two parameters are shown in Fig. 11 for one example of the power functional.

In the Hartree-Fock approximation, respectively, in the power functional with the collinear ansatz, the pair of bonding and antibonding orbitals that contribute to a natural orbital, given in Eq. (41), have the same spin direction. This results in the localization of the electron on one or the other site of the dimer. The emerging picture is appealing because it reflects the left-right correlations of the electrons. The admixture of antibonding states to the natural orbitals for the two spin directions is the same. Thus, there is no symmetry-breaking charge disproportionation.

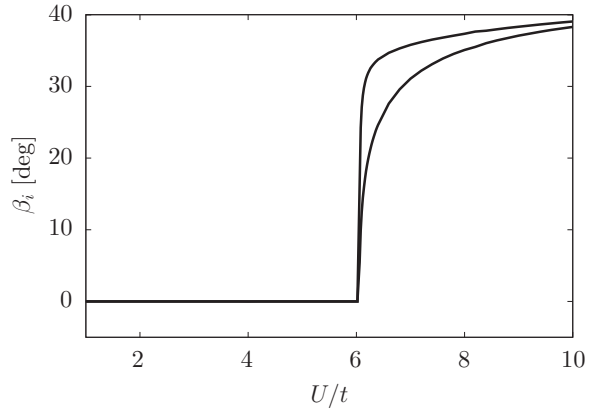

FIG. 11. Parameters β_1 and β_2 defining the natural orbitals Eq. (56) of the power functional for $\alpha = 0.53$ as a function of the interaction strength.

The natural orbitals Eq. (56) of the power functional are composed of bonding and antibonding orbitals with opposite spin directions. This leads to natural orbitals with equal weight on both sites, but the spins on both sides have a finite angle between them. The state has an intrinsically noncollinear, even though still a coplanar spin structure.

The admixture of antibonding states in the two pairs is independent in the power functional, so that the natural orbitals contain two independent free parameters, namely β_1 and β_2. The net magnetic moment of each of the four natural orbitals points along the same direction. For the choice in Eq. (56), this is the z direction. The parameters β_1 and β_2 control the relative angles of the local moments on the two sites of the dimer for each of the natural orbitals. This angle is $4\beta_1$ for the orbitals $|\phi_1^P\rangle$ and $|\phi_3^P\rangle$ and it is $4\beta_2$ for the orbitals $|\phi_2^P\rangle$ and $|\phi_4^P\rangle$. The natural orbitals are pairwise antiparallel: On any given site $|\phi_1^P\rangle$ and $|\phi_3^P\rangle$ have local moments in opposite directions. Similarly, this holds for $|\phi_2^P\rangle$ and $|\phi_4^P\rangle$.

It seems that the ground states of the power functional do not connect continuously to those of the Hartree-Fock approximation, because the natural orbitals belong to different classes. This is, however, not so: The ansatz for the natural orbital Eq. (56) connects smoothly to those of the Hartree-Fock approximation in Eq. (41) when the two parameters β_1 and β_2 become equal, and furthermore the occupations become integer. This limit of the ansatz Eq. (56) for the power functional describes, however, an antiferromagnet with the local moments aligned along the x direction, while the ansatz of Eq. (41) for the Hartree-Fock solution is polarized along the z direction. Thus they are related by a global spin rotation, which is a symmetry of the Hamiltonian.

VI. BEYOND HALF FILLING

Up to now, we considered only the half filled case of the Hubbard dimer. Here we consider also deviations from the particle number $N = 2$.

To avoid mathematical complications, we define $E(N)$ thermodynamically consistent as the zero-temperature limit of the Helmholtz potential $\beta \to \infty$, which in turn is constructed from the grand potential by a Legendre-Fenchel transform

$$E(N) = \lim_{\beta\to\infty} \max_{\mu} \left[-\frac{1}{\beta} \ln(\mathrm{Tr}\, \mathrm{e}^{-\beta(\hat{H}-\mu\hat{N})}) + \mu N \right]. \tag{57}$$

The trace is performed over the fermionic Fock space.

It can be shown that the total energy $E(N)$ consists of piecewise linear segments between integer particle numbers. Thus the slope of the total energy $E(N)$, the chemical potential $\mu = dE/dN$, is usually [45] discontinuous at integer occupations. This derivative discontinuity gives the fundamental band gap which is defined as the difference of electron affinity and ionization potential. The band gap is relevant, not only as an estimation related to optical spectra, but, more importantly, for the response functions and chemical equilibria. Therefore, we investigate whether the derivative discontinuities are properly described by the approximate density-matrix functionals.

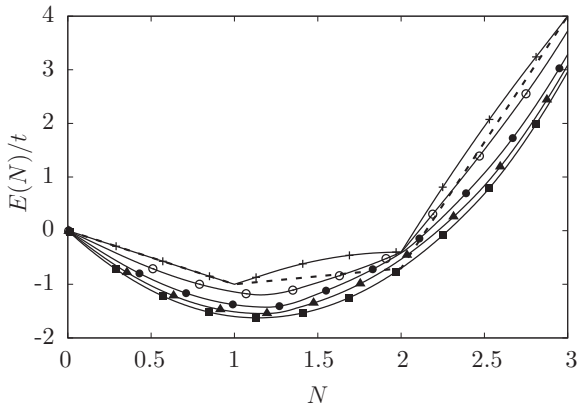

FIG. 12. Ground-state energy $E(N)$ of the Hubbard dimer with $U = 5t$ in units of the hopping parameter t as a function of particle number N. The critical power functional parameter for the transition to an antiferromagnetic state lies at $\alpha \approx 0.54$ for the given interaction strength. Dashed line: exact solution, crosses: Hartree-Fock approximation, open circles: power functional with $\alpha = 0.7$, filled circles: power functional with $\alpha = 0.58$, triangles: power functional with $\alpha = 0.53$, squares: Müller functional.

The total energy $E(N)$ of the exact solution and several power functionals is shown in Fig. 12 and the corresponding chemical potential in Fig. 13. For the Hubbard dimer, the derivative discontinuity at $N = 2$ is due to a combination of the one-particle gap and the interaction. The derivative discontinuity at $N = 1$ is, however, entirely due to the interaction. These features are clearly visible for the exact calculation shown in Fig. 12.

In the Hartree-Fock approximation, the energy for fractional occupations has a negative curvature for $1 < N < 3$. As a result, the derivative discontinuities are larger than in the exact solution. It reflects the well known observation that Hartree-Fock calculations overestimate band gaps. This observation can be rationalized with a lack of screening in the Hartree-Fock approximation that reduces the effective interaction strength.

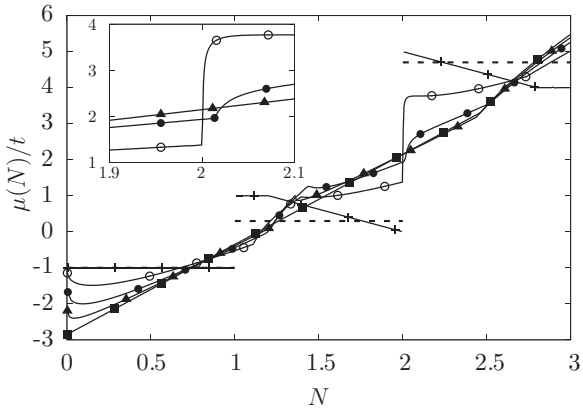

FIG. 13. Chemical potential $\mu(N)$ of the Hubbard dimer with $U = 5t$ in units of the hopping parameter t as a function of particle number N. The behavior of the power functional with $1/2 < \alpha < 1$ close to half filling is shown in the inset. Dashed line: exact solution, crosses: Hartree-Fock approximation, open circles: power functional with $\alpha = 0.7$, filled circles: power functional with $\alpha = 0.58$, triangles: power functional with $\alpha = 0.53$, squares: Müller functional.

The Müller functional, however, fails to give any derivative discontinuity. It is surprising that a functional that performs as well as the Müller functional for $N = 2$ is completely unable to capture the correct physics beyond half filling. It adds to the simplified picture that the Müller functional behaves very metal-like: It does not have a band gap and its magnetic susceptibility is infinite.

Except for the Hartree-Fock limit, also the power functional lacks a derivative discontinuity. This is apparent from Fig. 13. For small α, that is the Müller-like regime, the power functional behaves analogous to the Müller functional itself. In the parameter regime of the antiferromagnetic ground state, however, the chemical potential makes a continuous transition between two distinct linear functions of the particle number. This behavior of the power functional for the Hubbard dimer is analogous to that observed earlier for finite [46,47] and extended systems [25,48].

In order to extract values for the band gap despite the absence of a derivative discontinuity, Sharma *et al.* [25] proposed the extrapolation method, which exploits the behavior of $E(N)$ further away from the Fermi level. Sharma *et al.* exploit that the chemical potential makes a transition between two linear functions. The extrapolation of these linear functions to the integer particle number yields an offset which is identified with the band gap. This method yields finite band gaps in the appropriate parameter range of the power functional, where the Müller functional incorrectly predicts a vanishing band gap [25]. Surprisingly, the band gaps obtained using the extrapolation method from the power functional agree well with experimental results even for nonmagnetic calculations.

Our results for the Hubbard dimer shown in Fig. 13 indicate that the band gap obtained with the extrapolation method [25] can be tuned between zero and the Hartree-Fock value by adjusting α. Signatures of this behavior have been observed in studies that investigated the dependence on the power functional parameter α for realistic systems [25,47].

The absence of a true derivative discontinuity using the power functional and the tunability of the band gap determined with the extrapolation method is not limited to the antiferromagnetic ground state. As shown in Fig. 14, the Hubbard dimer behaves qualitatively similar, when the spin polarization is suppressed. In the nonmagnetic calculations, the onset of a finite band gap obtained by the extrapolation method is delayed to larger power parameters α. This finding is analogous to that observed for NiO, for which nonmagnetic calculations find a metallic ground state for $\alpha < 0.65$ [49], whereas noncollinear calculations find an insulating ground state already for $\alpha = 0.56$ [50].

VII. BEYOND THE DIMER

The question remains whether the findings for the Hubbard dimer persist in larger systems with more degrees of freedom. This is relevant for calculations of more complex systems having large unit cells. For this purpose we performed calculations for the power functional for Hubbard rings and Hubbard chains.

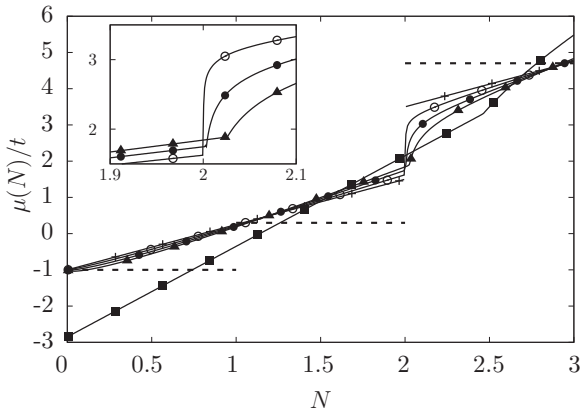

FIG. 14. Chemical potential $\mu(N)$ of the Hubbard dimer with $U = 5t$ in units of the hopping parameter t as a function of particle number N, when the density matrix is restricted to be nonmagnetic. The behavior of the power functional with $1/2 < \alpha < 1$ close to half filling is shown in the inset. Dashed line: exact solution, crosses: Hartree-Fock approximation, open circles: power functional with $\alpha = 0.95$, filled circles: power functional with $\alpha = 0.9$, triangles: power functional with $\alpha = 0.85$, squares: Müller functional.

Figure 15 shows the occupation numbers for a half-filled Hubbard ring at an intermediate interaction strength of $U = 5t$, which like the Hubbard dimer, has an antiferromagnetic ground state in the Hartree-Fock approximation. For the Müller functional we obtain fractional occupations as for the dimer. While the fractional occupations deviate from the exact result, their deviation from integer occupations are of the same order of magnitude as in the exact solution. The power functional exhibits abrupt transitions to an antiferromagnetic state around $\alpha_c \approx 0.58$ very analogous to the Hubbard dimer.

For a six-site Hubbard chain with seven electrons, i.e., one electron more than half filling, the pattern of transitions is even more complex: This behavior is shown in Figure 16. There are now three transitions:

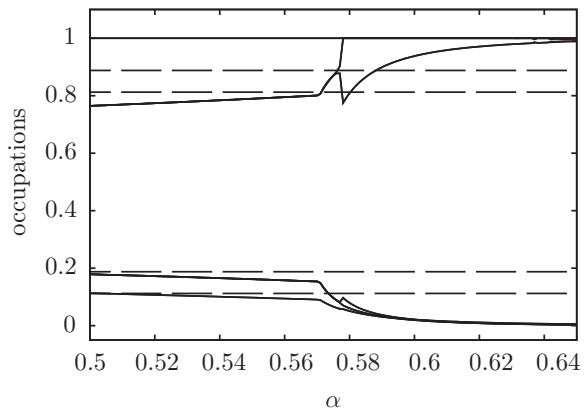

FIG. 15. Occupations of the half-filled six-site Hubbard-ring with $U = 5t$ for the power functional as a function of the parameter α (solid lines). The dashed horizontal lines indicate the occupations of the exact many-electron description. Evident are the rather abrupt transitions from fractional to integer occupations.

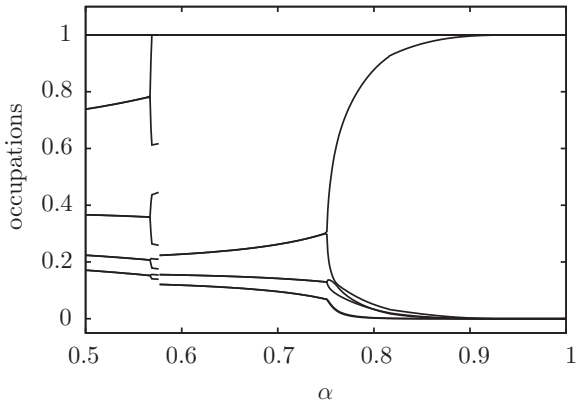

FIG. 16. Occupations of the six-site Hubbard-chain with seven electrons and $U = 5t$ for ground states of the power functional as function of the parameter α spanning the range from the Müller functional ($\alpha = 1/2$) to the Hartree-Fock approximation ($\alpha = 1$). Evident are the rather abrupt transitions from fractional to integer occupations.

(1) A continuous transition between $\alpha \approx 0.567$ and $\alpha \approx 0.569$ from the nonmagnetic Müller ground state to a state with collinear spins in the pattern $\uparrow\downarrow\uparrow\uparrow\downarrow\uparrow$, which is only stable in a small window of parameters.

(2) Around $\alpha \approx 0.576$ there is a nonsmooth transition to a state with an antiferromagnetic spin structure, i.e., $\uparrow\downarrow\uparrow\downarrow\uparrow\downarrow$.

(3) Beyond $\alpha \approx 0.75$, the antiferromagnetic structure breaks up and evolves into the HF-ground state having a spin structure given by $\uparrow\downarrow\uparrow\uparrow\downarrow\uparrow$.

These examples demonstrate that the power functional can generate a variety of magnetic states even for simple systems.

VIII. CONCLUSION

The popular density-matrix functionals, the Müller functional [22], the Hartree-Fock approximation and the power functional [25], which continuously interpolates between the other two, have been benchmarked for the Hubbard dimer. The Hartree-Fock approximation is, for the Hubbard model [14–16], analogous to hybrid density functionals [51], that admix a portion of exact exchange to the exchange-correlation energy. The local interaction of the Hubbard model acts analogous to the range separation [52,53], which suppresses the long-ranged Coulomb interaction in the Fock term. In this respect, the Hartree-Fock approximation also captures the main effects of the LDA+U method [7].

Particular emphasis has been given to left-right correlation, the dominant correlation effect for bond dissociation, which is not captured in local density functionals [5]. Left-right correlation describes that electrons localize on opposite sites of the dimer. This electron correlation, which increases with the interaction strength, avoids the energetic cost of the Coulomb repulsion due to double occupancy of a site. In the Hartree-Fock approximation, this left-right correlation leads to an antiferromagnetic state with a spin-up electron mostly localized on one side and the spin-down electron on the other. This so-called broken-symmetry state disagrees with the exact solution, which is a singlet state, having no local moments, but nevertheless antiferromagnetic correlations similar

to the broken symmetry state. More importantly, however, the antiferromagnetic transition is an abrupt one and not a continuous buildup of antiferromagnetic correlations as in the exact solution. The result is a qualitatively incorrect shape of the total energy during bond dissociation.

The Müller functional [22] establishes left-right correlation in a fundamentally different manner: while the natural orbitals are mostly—in the Hubbard dimer exactly—independent of the interaction, the occupations become fractional, which reflects the creation of electron-hole pairs that screen the interaction. One of the main successes of the Müller functional besides being able to produce fractional occupations correctly is that it captures the continuous nature of the transition to the left-right-correlated state.

Our calculations avoid any bias and allow for arbitrary noncollinear spin-polarized states. This strategy shall bring all potential problems to the surface that would be present in large scale electronic structure calculations using these density-matrix functionals.

Our first observation is that the ground state for the Müller functional, which does not have local moments, is degenerate with a one-dimensional manifold of ferromagnetic states. Thus the dimer has infinite magnetic susceptibility when described with the Müller functional, in contrast to the vanishing zero-temperature susceptibility of the exact solution of the Hubbard dimer. This large magnetic polarizability is likely to cause severe problems in extended electronic structure calculations.

When turning to the power functional [25], we find that the system behaves analogous to the Müller functional for small interactions, while it exhibits a transition to a Hartree-Fock-like antiferromagnetic state for large interactions. The critical interaction, where this transition occurs, drops rapidly with increasing α from infinity in the Müller functional to the Hartree-Fock value $U_{\mathrm{crit}} = 2t$. In the small-interaction regime the system is weakly pinned in the ferromagnetic state corresponding to the largest moment of the ground-state manifold of the Müller functional.

Our calculations indicate a major deficiency in the description of magnetic properties for this class of density-matrix functionals. The problems persist in modified form also for more general Hamiltonians, which include offsite Coulomb interactions, and for more extended systems.

Besides the bond-dissociation problem, we investigated the derivative discontinuity [5,54] with changing the number of electrons. A balanced description of the electron affinity and ionization potential is essential for a qualitatively correct description of charge transfer. We find that the metal-like behavior of the Müller functional persists: The discontinuity of the exchange-correlation energy even offsets the one of the kinetic energy. The Müller functional describes the Hubbard dimer with vanishing fundamental gap.

The power functional inherits many of the problems of the Müller functional: There is no derivative discontinuity in the entire parameter range of the power functional except for the Hartree-Fock limit. In the low-interaction regime the solutions are weakly ferromagnetic. Like the Hartree-Fock approximation, the power functional exhibits an artificial abrupt magnetic transition with increasing interaction towards an antiferromagnetic configuration, albeit at a larger critical interaction. These states are intrinsically noncollinear.

The absence of any derivative discontinuity also for insulating materials is expected to produce an artificial charge transfer between the constituents of large-scale electronic structure calculations. This cast severe doubt on the performance of such density-matrix functionals for complex systems.

While the power functional lacks a derivative discontinuity, its chemical potential undergoes a continuous transition between two linear functions, which has been exploited to extract a band gap from data obtained further away from the integer particle number [25,46–48].

Our calculations indicate, however, that the band gap obtained from this extrapolation can be tuned by the free parameter α of the power functional between zero and the Hartree-Fock result. The band gap opens in noncollinear calculations only when in the antiferromagnetic regime, while it vanishes in the Müller-type regime at low interactions. The opening of a band gap obtained by the extrapolation method and its tunability are features that persist in nonmagnetic calculations, while the gap opens at a larger value of the power parameter than in the magnetic calculation. These problems or signatures of them can be observed in previous calculations [25,31,47,49,50].

The tunability of the band gap is similar to other methods such as LDA+U [7] and hybrid density functionals [51]. However, the latter methods exhibit a true derivative discontinuity and their band gap does not shrink below the Kohn-Sham band gap, which is analogous to the noninteracting band gap of the Hubbard dimer.

Approximations for ionization potentials [55] and spectral functions [31] have been introduced on top of rDMFT. The latter method on the one hand yields spectra that agree well with experimental results for transition metal oxides [31,49,50] for particular choices of the power functional parameter. On the other hand investigations on the Hubbard dimer [30] suggest caution and claim that the underlying physics is not correctly treated.

The problems presented here demonstrate potential fundamental flaws of the class of density-matrix functionals of this study. We hope that this study provides a useful reference point for the development of new density-matrix functionals. We believe furthermore that our findings call for new approaches for the construction of density-matrix functionals that make closer contact to the many-particle description of the electronic system [20].

ACKNOWLEDGMENTS

We are deeply saddened by the loss of our dear colleague Thomas Pruschke. Financial support from the Deutsche Forschungsgemeinschaft through FOR1346 (project 9) is gratefully acknowledged.

[1] P. Hohenberg and W. Kohn, Phys. Rev. **136**, B864 (1964).
[2] W. Kohn and L. J. Sham, Phys. Rev. **140**, A1133 (1965).
[3] C. J. Cramer and D. G. Truhlar, Phys. Chem. Chem. Phys. **11**, 10757 (2009).

[4] U. von Barth, Phys. Scr. **2004**, 9 (2004).
[5] A. J. Cohen, P. Mori-Sánchez, and W. Yang, Chem. Rev. **112**, 289 (2012).
[6] K. Terakura, T. Oguchi, A. R. Williams, and J. Kübler, Phys. Rev. B **30**, 4734 (1984).
[7] V. I. Anisimov, J. Zaanen, and O. K. Andersen, Phys. Rev. B **44**, 943 (1991).
[8] A. Georges, G. Kotliar, W. Krauth, and M. J. Rozenberg, Rev. Mod. Phys. **68**, 13 (1996).
[9] K. Held, Adv. Phys. **56**, 829 (2007).
[10] G. Kotliar, S. Y. Savrasov, K. Haule, V. S. Oudovenko, O. Parcollet, and C. A. Marianetti, Rev. Mod. Phys. **78**, 865 (2006).
[11] J. Bünemann, W. Weber, and F. Gebhard, Phys. Rev. B **57**, 6896 (1998).
[12] T. Schickling, J. Bünemann, F. Gebhard, and W. Weber, New J. Phys. **16**, 093034 (2014).
[13] G.-T. Wang, X. Dai, and Z. Fang, Phys. Rev. Lett. **101**, 066403 (2008).
[14] M. C. Gutzwiller, Phys. Rev. Lett. **10**, 159 (1963).
[15] J. Hubbard, Proc. R. Soc. London A **276**, 238 (1963).
[16] J. Kanamori, Prog. Theor. Phys. **30**, 275 (1963).
[17] T. L. Gilbert, Phys. Rev. B **12**, 2111 (1975).
[18] M. Levy, Proc. Natl. Acad. Sci. USA **76**, 6062 (1979).
[19] P. E. Blöchl, C. F. J. Walther, and T. Pruschke, Phys. Rev. B **84**, 205101 (2011).
[20] P. E. Blöchl, T. Pruschke, and M. Potthoff, Phys. Rev. B **88**, 205139 (2013).
[21] J. M. Luttinger and J. C. Ward, Phys. Rev. **118**, 1417 (1960).
[22] A. M. K. Müller, Phys. Lett. **105**, 446 (1984).
[23] S. Goedecker and C. J. Umrigar, Phys. Rev. Lett. **81**, 866 (1998).
[24] O. Gritsenko, K. Pernal, and E. J. Baerends, J. Chem. Phys. **122**, 204102 (2005).
[25] S. Sharma, J. K. Dewhurst, N. N. Lathiotakis, and E. K. U. Gross, Phys. Rev. B **78**, 201103 (2008).
[26] M. A. L. Marques and N. N. Lathiotakis, Phys. Rev. A **77**, 032509 (2008).
[27] C. Benavides-Riveros and J. Várilly, Eur. Phys. J. D **66**, 274 (2012).
[28] N. N. Lathiotakis, S. Sharma, J. K. Dewhurst, F. G. Eich, M. A. L. Marques, and E. K. U. Gross, Phys. Rev. A **79**, 040501 (2009).
[29] T. Olsen and K. S. Thygesen, J. Chem. Phys. **140**, 164116 (2014).
[30] S. di Sabatino, J. A. Berger, L. Reining, and P. Romaniello, J. Chem. Phys. **143**, 024108 (2015).
[31] S. Sharma, J. K. Dewhurst, S. Shallcross, and E. K. U. Gross, Phys. Rev. Lett. **110**, 116403 (2013).
[32] D. J. Carrascal, J. Ferrer, J. C. Smith, and K. Burke, J. Phys. Condens. Matter **27**, 393001 (2015).
[33] P.-O. Löwdin, Phys. Rev. **97**, 1474 (1955).
[34] A. Coleman, Rev. Mod. Phys. **35**, 668 (1963).
[35] E. H. Lieb, Int. J. Quantum Chem. **24**, 243 (1983).
[36] T. Baldsiefen, A. Cangi, and E. K. U. Gross, Phys. Rev. A **92**, 052514 (2015).
[37] J. P. Perdew, K. Burke, and Y. Wang, Phys. Rev. B **54**, 16533 (1996).
[38] E. J. Baerends, Phys. Rev. Lett. **87**, 133004 (2001).
[39] M. Buijse and E. Baerends, Mol. Phys. **100**, 401 (2002).
[40] R. Car and M. Parrinello, Phys. Rev. Lett. **55**, 2471 (1985).
[41] J.-P. Ryckaert, G. Ciccotti, and H. J. C. Berendsen, J. Comput. Phys. **23**, 327 (1977).
[42] P.-O. Löwdin and H. Shull, Phys. Rev. **101**, 1730 (1956).
[43] Y. Suezaki, Phys. Lett. A **38**, 293 (1972).
[44] U. Bernstein and P. Pincus, Phys. Rev. B **10**, 3626 (1974).
[45] For degenerate states and when the electron addition and removal are dominated by delocalized states the discontinuity may also vanish or become infinitesimally small.
[46] N. Helbig, N. N. Lathiotakis, and E. K. U. Gross, Phys. Rev. A **79**, 022504 (2009).
[47] N. N. Lathiotakis, S. Sharma, N. Helbig, J. K. Dewhurst, M. A. L. Marques, F. Eich, T. Baldsiefen, A. Zacarias, and E. K. U. Gross, Zeitschrift fuer Physikalische Chemie **224**, 467 (2010).
[48] N. Helbig, N. N. Lathiotakis, M. Albrecht, and E. K. U. Gross, Europhys. Lett. **77**, 67003 (2007).
[49] Y. Shinohara, S. Sharma, S. Shallcross, N. N. Lathiotakis, and E. K. U. Gross, Journal of Chemical Theory and Computation **11**, 4895 (2015).
[50] Y. Shinohara, S. Sharma, J. K. Dewhurst, S. Shallcross, N. N. Lathiotakis, and E. K. U. Gross, New J. Phys. **17**, 093038 (2015).
[51] A. D. Becke, J. Chem. Phys. **98**, 1372 (1993).
[52] A. Savin, Int. J. Quantum Chem. Suppl. 22 **34**, 59 (1988).
[53] J. Heyd, G. Scuseria, and M. Ernzerhof, J. Chem. Phys. **118**, 8207 (2003).
[54] J. P. Perdew, R. G. Parr, M. Levy, and J. L. Balduz, Phys. Rev. Lett. **49**, 1691 (1982).
[55] K. Pernal and J. Cioslowski, Chem. Phys. Lett. **412**, 71 (2005).